A prediction of the longevity of the Lusi mud eruption, Indonesia

Maxwell L. Rudolph[a,*], Leif Karlstrom[a], Michael Manga[a,**]

[a]*Department of Earth and Planetary Science, University of California, Berkeley Berkeley, CA USA*

Abstract

A mud eruption, nicknamed Lusi, began near Sidoarjo, East Java, in May 2006. It has discharged $\sim 10^4 - 10^5$ m^3/day of mud ever since. In order to understand the nature of the eruption and its potential longevity, we develop a model for the coupled evolution of the mud source and ascent of mud through a conduit to the surface. The ascent of the mud is driven by overpressure in the mud source and by the exsolution and expansion of dissolved gases. We assume that erupted fluids originate in the mud source region. Mobilization of the mud is caused by elastic stresses induced by mud evacuation from the subsurface. We perform Monte Carlo simulations to explore model outcomes while perturbing the unknown material properties of the mud and surrounding medium. Using our preferred model, we calculate a 50% chance of the eruption lasting <41 years and a 33% chance that it lasts >84 years. Eruptions often end with the formation of a caldera, but longer eruptions are less likely to form a caldera. Model predictions can be refined with additional, but currently unavailable constraints: more precise estimates of

*Corresponding Author

**Principal Corresponding Author

Email addresses: rudolph@berkeley.edu (Maxwell L. Rudolph), manga@seismo.berkeley.edu (Michael Manga)

mud discharge, the yielding behavior of the materials in the subsurface, total gas content in the mud source, and identification of any erupted fluids that do not originate in the mud source.

---

1. Introduction

On 29th May, 2006 an eruption of mud and fluids occurred in Sidoarjo, Indonesia, creating a mud eruption named Lusi (short for Lumpur Sidoarjo). Approximately $10^4 - 10^5$ m^3/day of mud has erupted ever since (Mazzini et al., 2007), displacing >60,000 people (Bayuni, 2009). The large and active subsidence created by the eruption continues to damage transportation and communication infrastructure.

The birth and evolution of the Lusi eruption are well documented (Istadi et al., 2009; Mazzini et al., 2007) providing a special opportunity to study how and why large mud eruptions occur (Davies et al., 2007). Because the eruption occurred next to a 3 km deep gas exploration well, we also have unique insight into the subsurface lithology and properties immediately prior to the eruption. Specifically, we can constrain the source of the mud, origin of erupted fluids, and the driving mechanism of the eruption.

In this study, we develop a mechanical model for the Lusi eruption that couples mud transport to the surface through a conduit with the evolution of the mud source at depth. The model is analogous to those used for magmatic volcanoes in that there is a mud chamber and a conduit, and dissolved gases play a key role in sustaining the eruption. It differs in that the volume of mobilized mud (analogous to eruptible magma at a volcano) increases over time, owing to progressive mobilization of mud in the source region. We begin by summarizing some of

the key observations that guide model development. Next, we describe the model and governing equations. We end by predicting the longevity of the eruption and outline how to test and improve the model.

2. Observational Constraints

Microfossils imply a mud source in the upper Kalibeng formation, occurring at depths between 1220-1860 m, which consists of Pleistocene clay (Sawolo et al., 2009). The observed clay mineralogy is most similar to mud from 1600-1800 m (Mazzini et al., 2007). Kerogen compositions of erupted mud are also similar to those obtained from side-wall cores taken at a depth of 1707 m (Sawolo et al., 2009). Drilling logs indicate that the Kalibeng formation is under-compacted and over-pressured, with porosity of about 30% (Istadi et al., 2009; Tanikawa et al., 2010). There is some controversy over the porosity of the Kalibeng formation. Based on density logs from the well Banjar Panji-1 (BJP1) Davies et al. (2011a) estimate lower porosities (10-13%), which would necessitate an external water source.

While there is no debate about the source of mud, there is considerable disagreement about the source of fluid. The water content of the mud during the earliest stages of eruption was 60-70% (Mazzini et al., 2007; Istadi et al., 2009). This is greater than the porosity of the Kalibeng formation, $\sim$ 30%, implying an additional source of fluid. Davies et al. (2007) suggest that water is sourced from a carbonate aquifer at depths of 3 km. Mazzini et al. (2007) suggest that the primary source of water is diagenesis and dehydration within the source region of the erupted mud. The lower concentrations of B, Li, and Cl, as well as the δ^{18}O enrichment of the water, can be explained by clay dehydration. Carbon isotope

measurements of hydrocarbons and methane in the erupted mud indicate the presence of both biogenic methane, which could be produced in the source muds, and thermogenic methane, which, along with heavier hydrocarbons and H_2S, must have migrated from greater depths (Mazzini et al., 2007). The migration could have preceded the eruption.

The reported water content of the erupting mud provides an additional constraint. While the initial water content was high, 60-70% (Bayuaji et al., 2009), it gradually decreased to 30% over the first year (Mazzini et al., 2007). As this value is similar to the porosity of the source layer, we assume there is no significant addition of fluids to the mud source during the bulk of the eruption.

The temperature of the erupting mud is 70-100 °C (Sawolo et al., 2009). The geotherm measured in the BJP1 (~200 m from the site of the eruption) is 42°C/km and the mean annual air temperature is 27°C (Bayuaji et al., 2009); temperatures of 100 °C are reached at depths of 1700 m (Mazzini et al., 2007). The observed mud temperature does not require the addition of significant amounts of fluid hotter than the temperature at the source depth of the mud.

3. Model

We develop a model that is motivated and constrained by these observations. The fluids, mud and gas for the bulk of the eruption are sourced from the Kalibeng formation. Additional fluids may have played a key role in the initiation (Davies et al., 2007; Tingay et al., 2008) and during the early stages of the eruption, but will not influence subsequent dynamics, evolution, and longevity.

Our model is conceptually similar to typical models for magmatic volcanoes in that the system consists of a “chamber” coupled to a “conduit”. It differs, how-

ever, in the nature and origin of the chamber component as well as the boundary condition imposed on the conduit at the surface. For magmatic volcanoes and some mud volcano models (Zoporowski and Miller, 2009), the chamber boundary is a material surface and the chamber volume changes owing to influx or outflux during the eruption. In our model, an initially spherical chamber consists of mobilized mud – mud with a rheology that allows it to flow and to erupt. This chamber is surrounded laterally by mud of the same composition that has not yet become mobilized. The lateral extent of the mud chamber is therefore defined by a rheological, rather than a compositional, transition and evolves over time (Figure 1). Mud erupts through a cylindrical conduit, driven by gas exsolution and expansion and by chamber overpressure.

3.1. Mud Source

We model the mud chamber as a cylindrical cavity of thickness 600 m centered at a depth of 1500 m. The edges of the cavity are rounded (Figure 1), and the radius of curvature remains constant as the chamber expands. The details of the assumed chamber geometry (e.g. radius of curvature of the edges) are less important than the aspect ratio, which exerts the dominant control on the stress concentration near the lateral boundary of the chamber. For the purposes of calculating stresses outside the chamber, we assume that the continuum surrounding the chamber is a linear elastic solid over the time scale of the eruption. Stresses are governed by

$$\nabla \cdot \underline{\sigma} = \underline{0}, \tag{1}$$

where $\underline{\sigma}$ is the Cauchy stress, related to strain ($\underline{\epsilon}$) through the constitutive equation

$$\sigma_{ij} = \lambda \epsilon_{kk} \delta_{ij} + 2\mu \epsilon_{ij}. \tag{2}$$

Here λ and μ are the Lamé constants. The model domain is subject to stress boundary conditions at the chamber wall (∂S) and free surface ($z = 0$):

$$\sigma_n|_{\partial S} = \Delta P_C \tag{3}$$

$$\sigma_n|_{z=0} = \sigma_t|_{z=0} = 0. \tag{4}$$

Here σ_n and σ_t are the normal and tangential stresses, respectively. ΔP_C is equal to the difference between the current pressure in the mud source layer $P_C(t)$ and the initial source pressure, $P_C(0)$, and obeys the equation of state of the material in the chamber, described later. We calculate elastic stresses and strains numerically, using the axisymmetric program mode in FEAP, version 8.3 (Taylor, 2008). We assume an isotropic initial stress state, neglecting any effects arising from deviatoric tectonic stresses.

The equation of state relates specific volume v_S (volume per unit mass) of the 3-phase mixture inside the chamber to pressure P. If we denote the undeformed volume of the cavity $V_{0,C}$ and the deformed volume of the cavity V_C, the pressure satisfies

$$\rho_0 V_{0,C} + \int_0^t \dot{M}(\tau) d\tau = V_C(P)/v_S(P) \tag{5}$$

where $\dot{M}$ is the time derivative of chamber mass, which is the opposite of the eruptive mass discharge, and ρ_0 is the in-situ density of the mud at the initial chamber pressure. We perform Newton-Raphson iteration to obtain a chamber pressure that is consistent with the deformed volume of the cavity, the equation of state of the material inside the chamber, and the mass of material remaining in the chamber.

We adopt a von Mises yield stress (and equivalently, strain) criterion for mobilizing additional mud from the chamber's surroundings. The von Mises stress

is

$$\sigma_v = \sqrt{3J_2}, \tag{6}$$

where J_2 is the second deviatoric stress invariant. As mud erupts from the chamber, the chamber deflates and its pressure decreases, producing stresses in the surrounding mud. Once the von Mises stress in the unmobilized part of the mud layer exceeds a critical value $\sigma_{y,chamber}$ we assume that additional mud is mobilized and becomes part of the chamber. We solve for the expanding chamber radius iteratively so that the von Mises stress at the perimeter of the chamber is everywhere less than the yield stress. The von Mises stress criterion has been used to model mud yielding in other studies (e.g. Mazzini et al., 2009) and is the best higher-dimension analogue to the yielding criterion used to study mudflows in one dimension (e.g. Marr et al., 2002).

3.2. Conduit

Mud rises through a conduit towards the surface. The driving force is provided by a combination of mud chamber overpressure, and exsolution of dissolved gas and expansion of vapor during decompression and ascent. We model conduit processes assuming steady one-dimensional multiphase flow through a cylinder (e.g. Mastin, 2002; Dobran, 2001), subject to conservation of mass and momentum:

$$\frac{\partial}{\partial z}(\rho_{mix} u) = 0 \tag{7}$$

$$\frac{\partial P}{\partial z} = \frac{-\rho_{mix}\left(g + \frac{8\mu u}{\rho_{mix} r^2}\right)}{1 - \frac{u^2}{c^2}}. \tag{8}$$

In equations 7-8, u is the mixture velocity of mud plus gas, P is the pressure, g is gravity, μ is mud viscosity, r is the conduit radius. We note that the term $(8\mu u)/(\rho_{mix} r^2)$ can be interpreted as a friction factor, and any change to conduit

geometry (e.g. opening of multiple vents or widening/collapse of the main vent) would simply change the functional form of this term. ρ_{mix} is the mixture density, given by:

$$\rho_{mix} = \left(\frac{n}{\rho_g} + \frac{1-n}{\rho_l} \right)^{-1} \tag{9}$$

with n the mass fraction of gas, ρ_g and ρ_l the densities of gas and water plus particles respectively.

$$c = \left(\frac{\partial P}{\partial \rho_{mix}} \right)_S^{1/2} \tag{10}$$

is the sound speed of the mixture, calculated numerically to ensure mass conservation.

Equations 7-8 are solved with a bisection and shooting method and 4th order Runge-Kutta integration to satisfy two boundary conditions: a one-way coupling to the chamber pressure evolution at the base of the conduit

$$P(z = -H) = P_C \tag{11}$$

and an atmospheric pressure boundary condition at the surface

$$P(z = 0) = P_{atm} \tag{12}$$

We assume that gas bubbles are dynamically coupled to the flow until a critical porosity (gas volume fraction) of 0.3 is reached (Blower, 2001; Saar and Manga, 1999), which we take as the threshold permeability for gas loss. This limits the acceleration of mud in the conduit and effectively ensures that velocities never approach the sound speed of the mixture. We also assume that the water and mud particles are dynamically coupled. Tanikawa et al. (2010) estimate permeabilities of 10^{-20} to 10^{-19} m^2 in the Upper Kalibeng Formation. Assuming a driving

pressure gradient of 10 MPa/km (estimated from chamber overpressure and conduit length scale), we compute the pore fluid velocity as $v = -k/(\mu\phi)\nabla P = 10^{-12}$ m/s, many orders of magnitude smaller than the bulk velocity of the multiphase mixture.

The reservoir (chamber) enthalpy for a given initial temperature (T) and pressure (P) is calculated using the XSteam (www.x-eng.com) implementation of the International Association for the Properties of Water and Steam (IAPWS) IF-97 steam tables. We assume that the ascending mixture experiences isenthalpic decompression during transport (e.g. Lu and Kieffer, 2009), allowing us to calculate $T(z)$ from conservation of enthalpy and the steam tables. Once the P-T decompression path is known, we calculate the density and mass fraction of liquid and gas phases, which are functions of T and P, using the CH_4-H_2O equation of state developed by Duan et al. (1992a,b) and implemented in HCO-TERNARY (Nieva and Barragan, 2003) and the online calculator at geotherm.ucsd.edu. It is through this calculation that we account for changes in density due to gas exsolution and expansion, and we emphasize that the gas solubility is accounted for through the CH_4-H_2O equation of state and that the conversion of liquid water to vapor during ascent is limited by conservation of enthalpy.

4. Model Parameters

Our model contains a number of geometric and material properties, some that are well-constrained and others that are poorly constrained and treated as variables. The following have enough uncertainty to be treated as variables: failure strength of mud adjacent to the chamber ($\sigma_{y,chamber}$), failure strength of the near-surface material ($\sigma_{y,caldera}$), Young's modulus (E), and Poisson's ratio (ν).

4.1. Constants

Mud viscosity μ and conduit radius r affect mud ascent through the grouping μ/r^2. Manga et al. (2009) measured mud viscosity of 10^5 Pa·s on sample JV07-05 (Mazzini et al., 2007) of Lusi mud with 43 wt.% water. Water content has a large effect on viscosity. Rifai (2008) measured viscosity of samples collected from Lusi and found an approximately 80% increase in viscosity when water content decreased from 62.5 wt.% to 59.0 wt.%. Rudolph and Manga (2010) measured a fivefold increase in mud viscosity when water content decreased from 40 wt.% to 33 wt.%. The geometry of the conduit through which the mud rises cannot be observed directly. The initial fissure, observed within the first few days, was hundreds of meters long and tens of centimeters wide at the surface (Mazzini et al., 2007). Its burial by erupted mud does not allow us to determine how the conduit subsequently evolved and whether discharge became localized, as it does for magmatic fissure eruptions. In March 2007, 10 months after the eruption began, 40 cm diameter concrete balls were able to reach depths of 1000 m (Mazzini et al., 2007). As these balls had no effect on the eruption rate, their size provides a minimum estimate of conduit dimensions. For a given dissolved gas concentration, we choose a combined conduit dimension and viscosity that reproduces the observed 6×10^4 m^3/day mean discharge (Tingay, pers. comm. 2010), emphasizing again that viscosity and conduit radius enter the problem only through the grouping μ/r^2.

The volume ratio of erupted gases is spatially and temporally variable. Mazzini et al. (2007) measured gas composition at seeps near the crater and sampled steam clouds emanating from the crater. The seeps discharge 80-85% CH_4 and 10-19% CO_2. The gas samples from the steam cloud are more variable, with CO_2

comprising 28-74% and CH_4 comprising 24-72% of the gas among three samples. In general, the CO_2-enriched samples are also enriched in C_X for $X > 1$. We interpret these measurements as indicating a methane-dominated gas composition, following two lines of reasoning. First, CO_2 (specific gravity 1.53) and CX, X> 2 are denser than air while CH_4 is lighter than air (specific gravity 0.56). The steam samples were collected downwind of the crater, and some separation of gases by density may have occurred during transport. Second, we expect that the local gas seep chemistry, which is methane-rich, will be dominated by the composition of the erupting fluids. However, subsequent measurements may indicate that the erupting gas composition is CO_2-dominated (Mazzini, pers. comm. 2011). In our model, the gas composition is unimportant. As long as the discharge at initial chamber pressure fits the observational constraint, the relationship between chamber pressure and discharge is independent of gas composition. We show this graphically in Figure 2. The only discrepancy in cumulative mass removed (Figure 2) for the model using CO_2 and the model using CH_4 arises from a small mismatch in flux, less than 5%, the tolerance that we chose when calculating conduit velocities as a function of chamber pressure.

4.2. Unknowns

The value of $\sigma_{y,chamber}$ for the mud source is not known. Kopf et al. (2009) measured sediment shear strength in situ in the field (at the Dashgil mud volcano, Azerbaijan) using a Cone Penetration Test. They found strengths as low as 150 kPa in the conduit and 300-700 kPa at other locations. We thus consider values of $\sigma_{y,chamber}$ with a mean of 1 MPa for the pre-mobilized mud, and a standard deviation of an order of magnitude in log-space. Once the mud loses strength and enters the chamber or flows in the conduit, we treat it as a viscous fluid. The value

of $\sigma_{y,caldera}$ is also unknown, and we assume that it is 10 times larger than $\sigma_{y,chamber}$. We experimented with values of $\sigma_{y,caldera}/\sigma_{y,chamber}$ as large as 100 but found it to be unimportant. We explore a range of values for E (Young's modulus) and ν (Poisson's ratio) for the surroundings centered about 10^8 Pa and 0.15, respectively, chosen to be consistent with the geodetic modeling of Fukushima et al. (2009).

The mean values and range of parameters used in the Monte Carlo simulations are summarized in Table 1. We considered three scenarios. In the first, our preferred model, we give more weight to values of unknown parameters near our preferred mean value by using gaussian distribution of random numbers. E and $\sigma_{y,chamber}$ have values that are normally distributed in log-space, i.e. $\log_{10}\left(\sigma_{y,chamber}\ (\mathrm{Pa})\right) = 6 \pm 1$. We also performed the same suite of Monte Carlo simulations with probability density functions (pdfs) that are constant in the range $[mean - \sigma, mean + \sigma]$ or $[mean - 2\sigma, mean + 2\sigma]$ and zero elsewhere. We refer to these as σ-boxcar and 2σ-boxcar, respectively (Table 2).

5. Criteria to Terminate Eruption

The factors that cause eruptions to end are, in general, poorly understood. We consider two possible scenarios. First, the chamber pressure decreases (sometimes below lithostatic pressure) until there is insufficient potential energy available to drive the eruption. Alternatively, the eruption may end if the near-surface material fails, initiating caldera formation. The latter condition does not require that the eruption has ended, just that it has entered a regime in which our model is no longer applicable. Caldera formation occurs if continued removal of material induces failure of the overlying layers, and becomes more likely as the chamber grows and deviatoric stresses are concentrated between the surface and regions of

high curvature at the chamber walls. We evaluate J_2 (second deviatoric stress invariant) along a trajectory that begins at the tip of the mud chamber and progresses upward always in the direction of greatest J_2. We then evaluate J_2 along this trajectory at half the chamber depth. If the value at this point is greater than $\tau_{y,caldera}$, we assume that a caldera forms. This method produces a conservative criterion for caldera formation because J_2 is greatest at the free surface and decreases with increasing depth.

6. Results

To predict longevity, we performed Monte Carlo simulations in which we perturbed the four unknown model parameters. We illustrate the evolution of chamber pressure, chamber radius, total mass removed, and mass flux as a function of time during an individual Monte Carlo realization in Figure 2. Of 2584 simulations, 1223 eruptions ended due to chamber underpressure, 725 formed a caldera, 397 lasted longer than 100 years (the maximum time allowed for computational purposes), and 239 produced unbounded chamber growth (which is not geologically reasonable, as the mud source has finite lateral extent). In general terms, eruptions that ended due to insufficient chamber pressure never incorporated additional mud into the chamber because $\sigma_{y,chamber}$ was large; those that produced unbounded growth had the lowest $\sigma_{y,chamber}$. Caldera formation was favored by larger E and low $\sigma_{y,chamber}$. Our mean $E = 10^8$ Pa (Fukushima et al., 2009) and $\sigma_{y,chamber}$ lie close to the line that divides model outcomes in E-$\sigma_{y,chamber}$ space (Figure 3). Poisson's ratio is unimportant.

Although short eruptions are the most frequent model outcome, the observation that Lusi has been erupting for more than 4.5 years provides an additional

constraint. If we exclude all eruptions shorter than 4.5 years and give equal weight to all durations greater than 4.5 years, we obtain a cumulative probability distribution (Figure 4). The gaussian model predicts that the eruption has a 33% chance of lasting <21 years, a 50% chance of lasting less than 40 years, and a 67% chance of lasting <84 years. The σ-boxcar and 2σ-boxcar model results are summarized in Table 2.

7. Discussion

Eruptions driven by overpressure have approximately exponentially decaying discharge because the mass removal decreases overpressure (Woods and Huppert, 2003). In contrast, to date the Lusi eruption has displayed a remarkably uniform discharge, varying only by less than a factor of ten over the first few years. Eruption rates are difficult to determine accurately and the Lusi eruption is no exception. In the first few months discharge was about 50,000 m^3/day and increased to as much as 180,000 m^3/day over the next year (Mazzini et al., 2009). Satellite observations are most consistent with average eruption rates of 90,000 m^3/day (Istadi et al., 2009). Our model produces approximately constant eruption rates for a given conduit size because once the chamber begins expanding, the chamber pressure is buffered by incorporating additional material. Changes in observed eruption rates could reflect evolution of the conduit geometry or opening of new conduits, phenomena not captured by our model.

Mud volcanoes are known to form calderas (Kopf, 2008). Evans et al. (2008) describe mud calderas, both on land and submarine, with diameters of 1-2 km. Figure 3 shows that E and $\sigma_{y,chamber}$ are the key variables controlling caldera formation. Figure 5 is a histogram of eruption duration, also showing the breakdown

between eruptions that end due to chamber underpressure and eruptions culminating in the formation of a caldera. Eruptions that last longer are more likely to end due to chamber underpressure and less likely to form a caldera. Figure 6a is a histogram of caldera radii, which we assume to be equal to the chamber radius at the time of caldera formation. The calderas formed by our model most frequently have radii less than 2 km, although larger calderas can form. Figure 6b is a scatter plot of caldera radius as a function of time of formation. The positive-sloping trend of this plot implies that longer-lasting eruptions tend to form larger calderas, as expected.

There are two other models for the future of the Lusi eruption. The first, by Istadi et al. (2009) assumes an eruption rate and uses a GIS approach to account for subsidence and ponding of mud on the surface. As it does not address the controls of eruption rate and processes driving the mud to the surface we do not discuss it further. This model does, however, address a feature of the eruption that we neglect, namely the emplacement and redistribution of the mud after eruption.

Davies et al. (2011b) develop a model that is more similar in approach to our own in that they model the mechanics of the eruption process and mass transport. The model differs significantly, however, in the inferred source of the fluids that mix with the mud, the plumbing system for the fluids and mud, and the driving forces for the eruption. Davies et al. (2011b) assume that water from a deep artesian carbonate aquifer flows upwards into the 15 cm-diameter borehole created by drilling operations. At the depths of the mud source, 1.8-1.6 km, the water exits the conduit, mixes with mud in something analogous to our mud chamber, and then erupts. The driving mechanism is overpressure in the carbonate aquifer, and water from this aquifer entrains mud and carries it to the surface. Our model

thus differs conceptually in two important respects: the importance of the deep carbonate aquifer, and the driving forces. We have argued that a source of extra fluid is not needed after the initial phases of the eruption. Without this additional source of overpressure, our eruption is sustained by exsolution and expansion of gases derived from the mud source region. We note that the 50th percentile eruption duration predicted by Davies et al. (2011b) is 26 years, substantially less than we predict without invoking an external fluid source. We expect that the addition of an external source of fluids (and overpressure) to our model would increase the duration of our model eruptions.

8. Conclusions

In summary, we considered two possible scenarios under which the current eruption may end, either through the eventual inability of dissolved gases to sustain the eruption, or the formation of a caldera. We made some necessary simplifications in order to develop a tractable model, most importantly the assumption of constant conduit geometry and uniform material properties of the mud source and surroundings. There is also considerable uncertainty in mechanical properties such as viscosity, failure strength of the mud, initial gas content, and origin of additional fluids. However, once we constrain the model to produce the observed eruption rate, uncertainty in viscosity and gas content have little effect on longevity predictions.

Validating our conceptual model is necessary for its predictions to be relevant and useful for planning. It should be possible to demonstrate the existence and amount of additional fluids (Davies et al., 2007, 2011b) by sampling fluids from the mud source and deeper aquifers, and comparing these with samples of the

erupted mud. There is also some ambiguity in the measurements of gas composition, and the collection of gas samples directly from Lusi's crater would better inform our model parameters. We have also neglected to include aspects of regional tectonics that may influence the eruption, particularly if the mud source expands. Perhaps most important is the role of stresses from the reactivated Watukosek fault that passes through the eruption source (Mazzini et al., 2009). The spatial correlation of mud volcano locations with the fault suggests that the fault influences at least the location of the eruptions. Our treatment of mud rheology and mobilization is simplified, as mud failure and flow are complicated. Finally, our treatment of the region surrounding the mud chamber as elastic cannot account for surface cracks and motion on nearby faults, features that suggest brittle failure or plastic deformation. Despite the uncertainties in material properties and the model approximations, our modeling framework allows us to make probabilistic estimates of longevity and to highlight how predictions can be improved in light of better observational constraints.

Acknowledgements

This work was supported by the National Science Foundation under Grant No. EAR-1114184. We thank A. Mazzini for providing mud samples and R. Swarbrick and R. Davies for discussions and for sharing their work. M.L.R. is supported by a Graduate Research Fellowship from the National Science Foundation. We thank Adriano Mazzini and two anonymous reviewers for comments that substantially improved the quality of the manuscript.

Abidin, H.Z., Davies, R.J., Kusuma, M.A., Andreas, H., Deguchi, T., 2008. Subsidence and uplift of Sidoarjo (East Java) due to the eruption of the Lusi mud volcano (2006-present). Environ. Geol. 57(4), 833-844.

374 Bayuaji, L., Watanabe, H., Tonooka, H., Sumantyo, J.T.S., Kuze, H. Study on land
375 surface temperature characteristics of ho mud eruption in East Java, Indonesia.
376 Intl. J. Rem. Sens. Earth Sci. 6, 14-28.

377 Bayuni, E.M., 2009, December 1. Lusi spurs geologists interest. The Jakarta
378 Post. Retrieved from http://www.thejakartapost.com/news/2009/12/01/lusi-
379 spurs-geologists-interest.html.

380 Blower, J.D., 2001. Factors controlling permeability-porosity relationships in
381 magma. Bull. Volcanol. 63, 497-504.

382 Davies, R.J., Swarbrick, R.E., Evans, R.J., Huuse, M., 2007. Birth of a mud vol-
383 cano: East Java, 29 May 2006. GSA Today 17, 4-9.

384 Davies, R.J., Manga, M., Tingay, M., and Swarbrick, R., 2011. Fluid
385 transport properties and estimation of overpressure at the Lusi mud vol-
386 cano, East Java Basin (Tanikawa et al., 2010). Engineering Geology,
387 doi:10.1016/j.enggeo.2011.03.010.

388 Davies, R.J., Mathias, S.A., Swarbrick, R.E., and Tingay, M.J., 2011. Probabilistic
389 longevity estimate for the LUSI mud volcano, East Java. J. Geol. Soc. Lond.
390 168, 1-7.

391 Dobran, F., 2001. Volcanic processes: mechanisms in material transport. Kluwer
392 Academic, New York USA.

393 Duan, Z., Moller, N., Weare, J.H., 1992. An equation of state for the CH_4-CO_2-
394 H_2O system: I. Pure systems from 0 to 1000°C and 0 to 8000 bar. Geochim.
395 Cosmochim. Acta 56, 2605-2617.

Duan, Z., Moller, N., Weare, J.H., 1992. An equation of state for the CH_4-CO_2-H_2O system: II. Mixtures from 50 to 1000°C and 0 to 8000 bar. Geochim. Cosmochim. Acta. 56, 2619-2631.

Evans, R.J., Stewart, S.A., Davies, R.J., 2008. The structure and formation of mud volcano summit calderas. J. Geol. Soc. 165(4), 769-780.

Fukushima, Y., Mori, J., Hashimoto, M., Kano, Y., 2009. Subsidence associated with the Lusi mud eruption, East Java, investigated by SAR interferometry. Mar. Pet. Geol. 26(9), 1740-1750.

Istadi, B., Pramono, G.H., Sumintadireja, P., Alam, S., 2009. Modeling study of growth and potential geohazard for LUSI mud volcano: East Java, Indonesia. Mar. Pet. Geol. 26(9), 1724-1739.

Kopf, A.J., 2008. Volcanoes: Making calderas from mud. Nature Geosci. 1(8), 500-501.

Kopf, A., Stegmann, S., Delisle, G., Panahi, B., Aliyev, C.S., Guliyev, I., 2009. In situ cone penetration tests at the active Dashgil mud volcano, Azerbaijan: Evidence for excess fluid pressure, updoming, and possible future violent eruption. Mar. Pet. Geol. 26(9), 1716-1723.

Lu, X., Kieffer, S., 2009. Thermodynamics and mass transport in multicomponent, multiphase H2O systems of planetary interest. Ann. Rev. Earth Planet. Sci. 37, 449-477.

Manga M., Brumm M., Rudolph, M.L., 2009. Earthquake triggering of mud volcanoes. Mar. Pet. Geol. 26(9), 1785-1798.

Marr, J. G., Elverhøi, A., Harbitz, C., Imran, J., Harff, P., 2002. Numerical simulation of mud-rich subaqueous debris flows on the glacially active margins of the Svalbard-Barents Sea. Mar. Geol., 188(3-4), 351364.

Mastin, L., 2002. Insights into volcanic conduit flow from an open-source numerical model. Geochem. Geophys. Geosyst. 3(7), 1037.

Mazzini, A., Svensen, H., Akhmanov, G., Aloisi, G., Planke, S., Malthe-Sørenssen, A., Istadi, B., 2007. Triggering and dynamic evolution of Lusi mud volcano, Indonesia. Earth Planet. Sci. Lett. 261, 375388.

Mazzini, A., Nermoen, A., Krotkiewski, M., Podladchikov, Y., Planke, S., Svensen, H., 2009. Strike-slip faulting as a trigger mechanism for overpressure release through piercement structures. Implications for the Lusi mud volcano, Indonesia. Mar. Pet. Geol. 26(9), 1751-1765.

Nieva, D., Barragan, R.. 2003. HCO-TERNARY: A FORTRAN code for calculating P-V-T-X properties and liquid vapor equilibria of fluids in the system H2O-CO2-CH4. Computers and Geosciences 29(4):469-485.

Rifai, R., 2008. Spatial modelling and risk assesment of Sidoarjo mud volcanic flow. M. Sc. Thesis, Gadjah Mada University.

Rudolph, M.L., Manga, M., 2010. Mud volcano response to the 4 April 2010 El Mayor-Cucapah earthquake. J. Geophys. Res. 115, B12211.

Saar, M.O., Manga, M., 1999. Permeability-porosity relationship in vesicular basalts. Geophys. Res. Lett. 26(1), 111-114.

Sawolo, N., Sutriono, E., Istadi, B.P., Darmoyo, A.B., 2009. The LUSI mud volcano triggering controversy: Was it caused by drilling? Mar. Pet. Geol. 26(9), 1766-1784.

Tanikawa, W., Sakaguchi, M., Wibowo, H.T., Shimamoto, T., Tadai, O., 2010. Fluid transport properties and estimation of overpressure at the Lusi mud volcano, East Java Basin. Eng. Geol. 116(1-2), 73-85.

Taylor, R.L., 2008. FEAP: A Finite Element Analysis Program. User Manual.

Tingay, M.R.P., Heidbach, O., Davies, R., Swarbrick, R.E., 2008. Triggering of the Lusi mud eruption: earthquake versus drilling initiation. Geology 36, 639-642.

Woods, A.M., Huppert, H.E., 2003. On magma chamber evolution during slow effusive eruptions. J. Geophys. Res. 108(B8), 2403.

Zoporowski, A., Miller, S.A., 2009. Modelling eruption cycles and decay of mud volcanoes. Mar. Pet. Geol. 26(9), 1879-1887.

Symbol	Value (or Mean)	Standard Deviation	Description
$\log_{10}$(E (Pa))	8	1	Young's modulus
ν	0.15	0.1	Poisson's ratio
$\log_{10}(\sigma_{y,chamber}$(Pa))	6	1	Yield strength of mud source layer
$\sigma_{y,caldera}$	10 $\sigma_{y,chamber}$	N/A	Yield strength of near-surface material
μ	10^4 Pa s	N/A	Viscosity in conduit
r	1.4 m	N/A	Conduit radius
[CH_4]	0.5 wt %	N/A	Methane mole fraction
[CO_2]	1 wt %	N/A	CO_2 mole fraction

Table 1: Summary of the values for model parameters. The means and standard deviations listed were used in our Monte Carlo simulations.

Prior PDF Shape	Gaussian	σ boxcar	2σ boxcar
33% Longevity (years)	21	27	14
50% Longevity (years)	40	50	25
75% Longevity (years)	84	>100	52

Table 2: Summary of model results for both choices of gas composition and different assumptions about the distribution of model unknowns. Models with gaussian pdfs use the means and standard deviations shown in Table 1. Models with σ-boxcar and 2σ-boxcar distributions use mean values and standard deviations (σ) from Table 1 and assume a flat pdf within σ or 2σ of the mean.

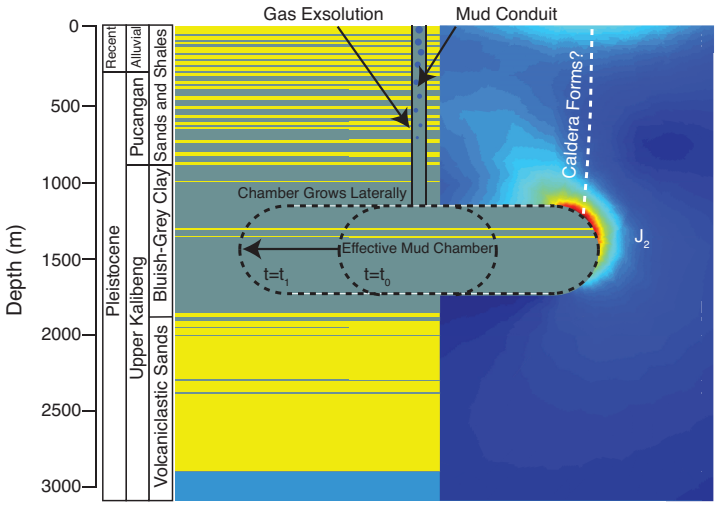

Figure 1: An illustration of model geometry and how it relates to subsurface lithology, (left of conduit) and our calculated J_2 (second deviatoric stress invariant), right of conduit. Warmer colors indicate larger values of J_2. Stratigraphy is adopted from (Mazzini et al., 2007) and is based on logs of BJP1.

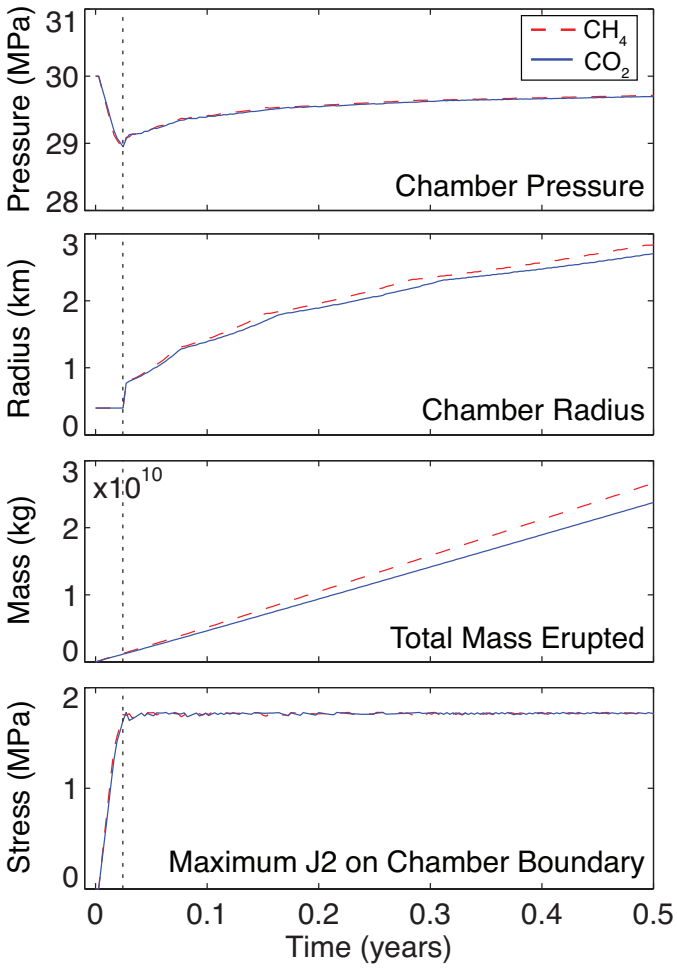

Figure 2: Temporal plots of chamber pressure, chamber (mobilized region) radius, cumulative mass erupted, and maximum J_2 on the chamber boundary (top to bottom). The red dashed lines are from a model in which we used 0.5 mol % CH_4 while the blue curves are for a model with 1 mol % CO_2. The two models are otherwise identical. The most important feature of the model results, illustrated here, is that once yielding begins (indicated by dashed vertical line), there is a drastic change in system behavior. Chamber radius begins to increase, and chamber pressure is buffered by the incorporation of material with higher pore pressure than that of the material filling the chamber prior to expansion. Like chamber pressure, mass flux is buffered and varies only by about 1% and J_2 remains constant at the value of the yield strength ($\tau_{y,chamber}$).

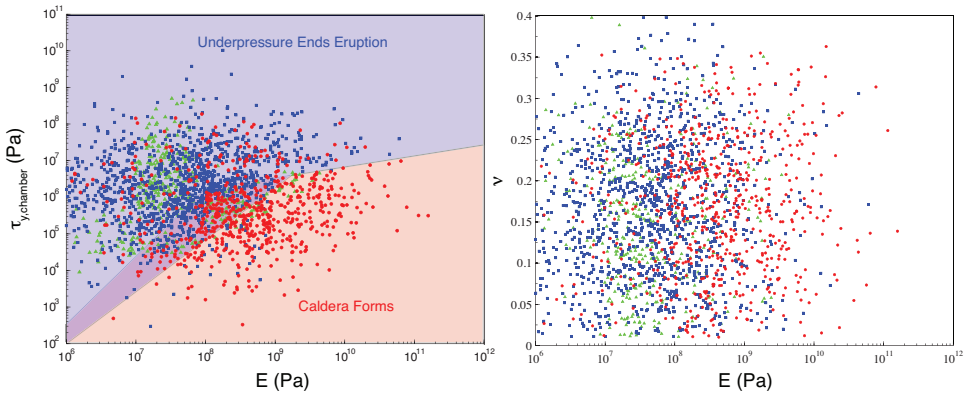

Figure 3: Regime diagram illustrating effect of variables on model outcome (gaussian model). Each glyph represents one model realization and colors/shapes correspond to outcomes: blue squares - insufficient chamber pressure ends eruption, red circles - caldera forms, green triangles - eruption lasts longer than 100 years.

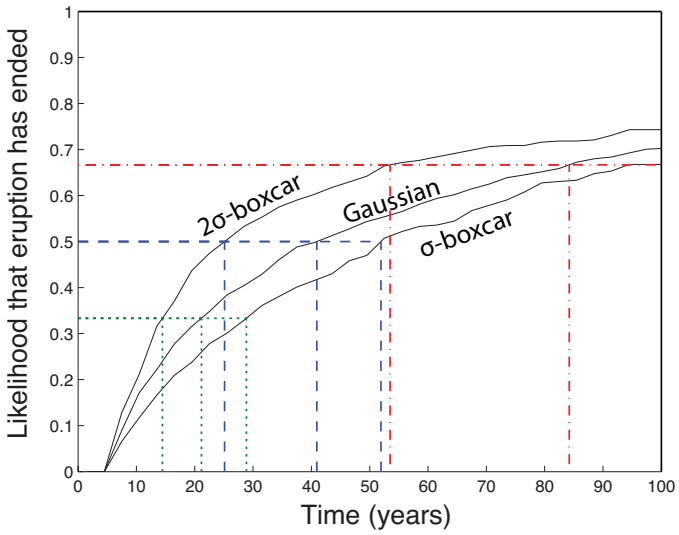

Figure 4: Cumulative probability that the eruption has ended for all three distributions of unkown variables. Horizontal axis is time since eruption started, vertical axis is likelihood that eruption will have ended or formed a caldera. Green dotted, blue dashed, and red dot-dashed lines indicate times at which likelihood is $1/3$, $1/2$, and $2/3$, respectively.

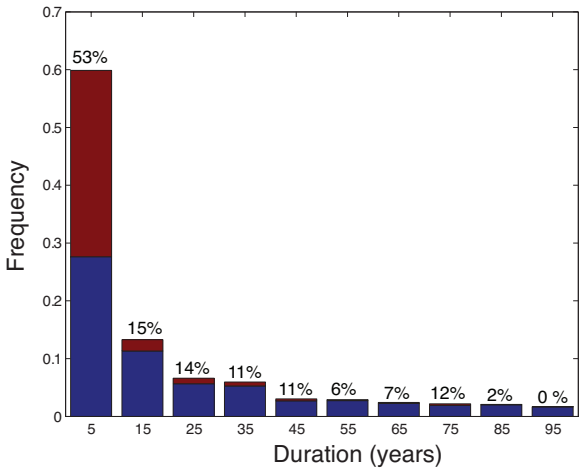

Figure 5: Histogram of eruption durations for gaussian model. Red bars indicate eruptions that formed a caldera and blue bars indicate eruptions that ended due to insufficient chamber pressure. We list the percentage of the eruptions in a given bin that ended due to caldera formation.

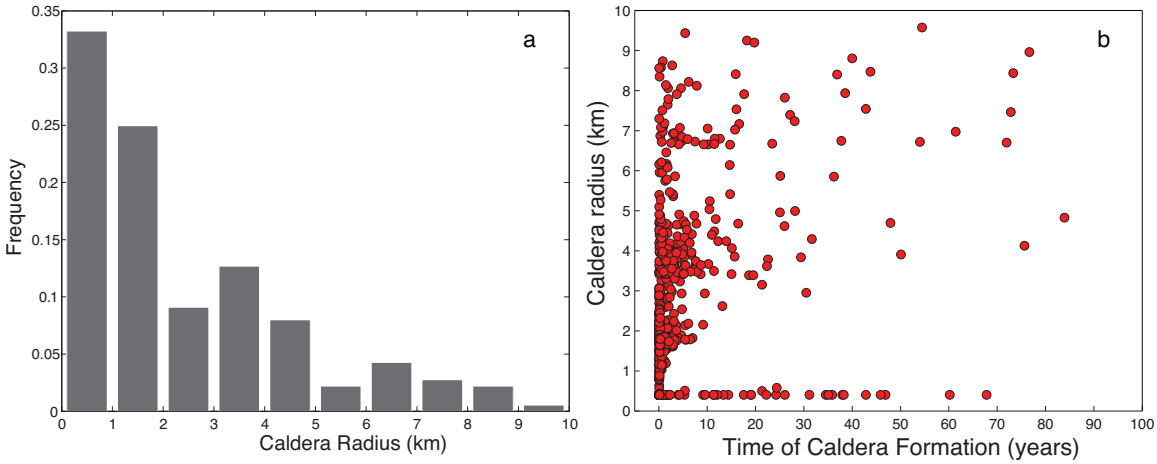

Figure 6: (a) Histogram of caldera radii for gaussian model. Frequency of radii of caldera formed in the model, normalized so that bins sum to 1. (b) Relationship between caldera radius and time of formation.